Interactive Entanglement in Hybrid Opto-magno-mechanics System

Jun Wang[1], Jing-Yu Pan[1], Ya-Bo Zhao[1], Jun Xiong[1] and Hai-Bo Wang[1*]

[1]Department of Physics, Beijing Normal University, Beijing, 100875, China.

*Corresponding author(s). E-mail(s): hbwang@bnu.edu.cn;

Abstract

We present a novel cavity opto-magno-mechanical hybrid system to generate entanglements among multiple quantum carriers, such as magnons, mechanical resonators, and cavity photons in both the optical and microwave domains. Two Yttrium iron garnet (YIG) spheres are embedded in two separate microwave cavities which are joined by a communal mechanical resonator. Because the microwave cavities are separate, the ferromagnetic resonate frequencies of two YIG spheres can be tuned independently, as well as the cavity frequencies. We show that entanglement can be achieved with experimentally reachable parameters. The entanglement is robust against environmental thermal noise, owing to the mechanical cooling process achieved by the optical cavity. The maximum entanglement among different carriers is achieved by optimizing the parameters of the system. The individual tunability of the separated cavities allows us to independently control the entanglement properties of different subsystems and establish quantum channels with different entanglement properties in one system. This work could provide promising applications in quantum metrology and quantum information tasks.

Keywords: Entanglement, Optomechanics, Magnonics, Quantum Information

1 Introduction

Quantum entanglement is the key resourse for quantum information science, such as quantum computing[1–4], quantum key distribution[5, 6], quantum

secret sharing [7–9], quantum teleportation [10], quantum dense coding[11], quantum secure direct communication[12, 13], and so on. Entanglement has been generated in many systems such as photons[14], atoms[15], and superconductors[16]. To coherently couple different quantum systems, mechanical oscillators have been widely used [17, 18], which lead to the development in the research area known as optomechanics. Ferromagnetic systems, which have been widely studied since 1946[19–21], provide an alternative way to couple different quantum information carriers. Strong coupling between the collective excitation of magnetization in ferrimagnetic materials (which is known as magnon) and photon inside microwave (MW) cavity has been achieved[22, 23]. Yttrium iron garnet (YIG, $Y_3Fe_5O_{12}$) is an excellent ferrimagnetic material for quantum information processing, owing to its very high spin density and low loss[24, 25]. YIG sphere inside the MW cavity provides strong coupling between magnons and cavity photons near the resonance point, which can be flexibly tuned by adjusting the bias magnetic field. Meanwhile, a membranous mechanical resonator can be coupled to a MW cavity as a vibrating capacitor[26–28]. In addition, direct coupling between magnons and vibration modes of YIG sphere can be achieved by magnetostrictive interaction[29]. These magnon-photon-phonon hybrid systems provide a privileged platform for coherently transferring quantum states among different systems.

The entanglement properties of hybrid opto-magno-mechanical systems have been widely studied at both mean field level[29] and full quantum level[30]. Several protocols to generate entanglement among cavity magnomechanics system have been reported [31–37]. Schemes to entangle two YIG spheres in a single cavity have been proposed in previous work[33], but to entangle YIG spheres in separate cavities is still a pending problem. The use of separated cavities will make it more convenient to study the frequency-tunable characteristics of entanglement among YIG spheres and MW cavities.

Distinguished from all previous approaches, we present a hybrid opto-magno-mechanical system that includes two magnons embedded in two separate MW cavities, a mechanical oscillator, and an ancilla optical cavity. Because the microwave cavities are separate, the ferromagnetic resonate frequencies of two YIG spheres can be tuned independently, as well as the cavity frequencies. Entanglements are generated by the nonlinearity of the system such as the magnetic dipole interaction and radiation pressure. Meanwhile, the mechanical oscillator is cooled by the ancilla optical cavity, which plays an important role in obtaining steady state and decresing thermal noise. We consider the quantum fluctuations and solve the system via linearized quantum Langevin equations. We calculate the entanglement properties by solving the Lyapunov equation and calculating the logarithmic negativity[38–40]. The results show that our model can yield strong entanglements by optimizing the detunings between driven fields and cavities or magnons. The individual tunability of the separated cavities allows us to independently control the entanglement properties of different subsystems and establish quantum channels with different entanglement properties in one system. Besides, the

entanglements are robust against environmental temperature at the millikelvin level.

2 The Model
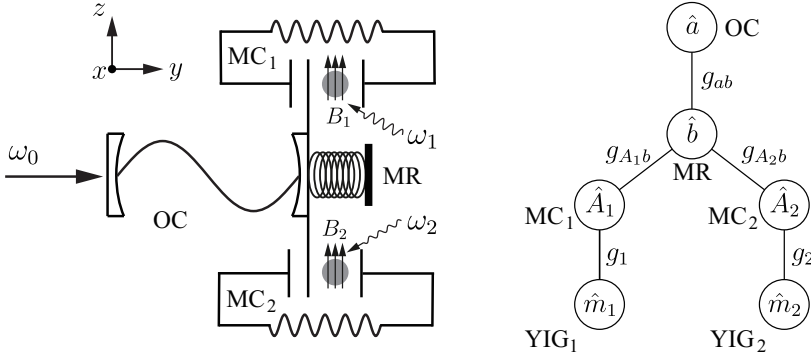
Fig. 1 Schematic diagram. A mechanical resonator (MR) is coupled to an optical cavity (OC) and two microwave cavities (MCs). An yttrium iron garnet (YIG) sphere is embedded at the magnetic-field antinode of the microwave cavity. The YIG spheres inside MCs are driven by microwaves ω_1 and ω_2 respectively. At the position of the YIG sphere, the bias magnetic field is along the z direction, the driving magnetic field is along the y direction, and the magnetic field of the cavity mode is along the x direction.

The magnon-photon-phonon coupling system is shown in Fig.1. A communal mechanical resonator (MR) is coupled to an optical cavity (OC) and capacitively coupled to two microwave cavities (MC)[26–28]. An yttrium iron garnet (YIG) sphere is embedded in each microwave cavity. The resonate frequencies of OC and two MCs are ω_a, ω_{A1}, and ω_{A2}, respectively. The ferromagnetic resonate frequencies of two YIG spheres are ω_{m_1} and ω_{m_2}, which can be tuned by the static bias magnetic field B_j (j = 1, 2) via $\omega_{m_j} = \gamma B_j$ ($\gamma/2\pi$ = 28GHz/T is the gyromagnetic ratio). The MR couples with cavity fields through radiation pressure interaction, with coupling rates g_{ab} (MR-OC), g_{A1b} (MR-MC1), and g_{A2b} (MR-MC2). The magnons inside MCs couple with cavity fields through magnetic dipole interaction, with coupling rates g_1 and g_2. The OC is driven by an optical field ω_0, while the YIG spheres inside MCs are driven by microwaves ω_1 and ω_2 respectively. The direct coupling between the YIG sphere and the microwave driving field is adopted in previous work [30, 41, 42]. The decay rates of OC, two MCs, and two magnons are κ_a, κ_{A_i}, and κ_{m_i} (i=1,2). The total Hamiltonian is:

$$
\begin{aligned}
H = &\hbar\omega_a a^\dagger a + \hbar \sum_{i=1,2} (\omega_{m_i} m_i^\dagger m_i + \omega_{A_i} A_i^\dagger A_i) + \hbar\omega_b b^\dagger b - g_{ab} a^\dagger a (b + b^\dagger) \\
&+ \hbar \sum_{i=1,2} [g_i(A_i + A_i^\dagger)(m_i + m_i^\dagger) - g_{Aib} A_i^\dagger A_i (b + b^\dagger)]
\end{aligned}
$$

$$+ i\hbar\Omega_0(a^\dagger e^{-i\omega_0 t} - ae^{i\omega_0 t}) + i\hbar \sum_{i=1,2} \Omega_i(m_i^\dagger e^{-i\omega_i t} - m_i e^{i\omega_i t}), \qquad (1)$$

where $a(a^\dagger)$, $b(b^\dagger)$, $A_i(A_i^\dagger)$, and $m_i(m_i^\dagger)$ are the creation (annihilation) operators for the optical cavity mode, the mechanical mode, the i-th microwave cavity mode, and the i-th magnon mode, respectively. The Rabi frequencies Ω_0, Ω_1, and Ω_2 denote the strength of the driven fields ω_0, ω_1, and ω_2, respectively.

In the rotating frame with respect to $\omega_0 a^\dagger a + \omega_1 m_1^\dagger m_1 + \omega_2 m_2^\dagger m_2 + \omega_1 A_1^\dagger A_1 + \omega_2 A_2^\dagger A_2$ and applying the rotating-wave approximation $(A_i + A_i^\dagger)(m_i + m_i^\dagger) \approx A_i m_i^\dagger + A_i^\dagger m_i$ (when $\omega_{A_i}, \omega_{mi} \gg g_i, \kappa_{A_i}, \kappa_{m_i}$), the effective Hamiltonian is:

$$H = \hbar\Delta_{a_0} a^\dagger a + \hbar \sum_{i=1,2} (\Delta_{m_i} m_i^\dagger m_i + \Delta_{A_i} A_i^\dagger A_i) + \hbar\omega_b b^\dagger b - g_{ab} a^\dagger a(b + b^\dagger)$$

$$+ \hbar \sum_{i=1,2} [g_i(A_i m_i^\dagger + A_i^\dagger m_i) - g_{A_i b} A_i^\dagger A_i(b + b^\dagger)] + i\hbar\Omega_0(a^\dagger - a)$$

$$+ i\hbar \sum_{i=1,2} \Omega_i(m_i^\dagger - m_i), \qquad (2)$$

where $\Delta_{a_0} = \omega_a - \omega_0$, $\Delta_{mi} = \omega_{m_i} - \omega_i$, and $\Delta_{Ai} = \omega_{A_i} - \omega_i$ denote the detunings of the driven fields. The quantum Langevin equations (QLEs) of the system are:

$$\dot{a} = -(i\Delta_{a_0} + \kappa_a)a + ig_{ab}(b + b^\dagger)a + \Omega_0 + \sqrt{2\kappa_a}a^{in}, \qquad (3)$$

$$\dot{b} = -(i\omega_b + \kappa_b)b + ig_{ab}a^\dagger a + ig_{A_1 b}A_1^\dagger A_1 + ig_{A_2 b}A_2^\dagger A_2 + \sqrt{2\kappa_b}b^{in}, \qquad (4)$$

$$\dot{m}_i = -(i\Delta_{m_i} + \kappa_{m_i})m_i - ig_i A_i + \Omega_i + \sqrt{2\kappa_{m_i}}m_i^{in}, \qquad (5)$$

$$\dot{A}_i = -(i\Delta_{A_i} + \kappa_{A_i})A_i + ig_{A_i b}(b + b^\dagger)A_i - ig_i m_i + \sqrt{2\kappa_{A_i}}A_i^{in}, \qquad (6)$$

where a^{in}, b^{in}, m_i^{in}, and A_i^{in} are input noise operators for the optical cavity mode, the mechanical mode, the magnon modes, and the microwave cavity modes, respectively, which are characterized by the following correlation functions:

$$\langle a^{in}(t)a^{in\dagger}(t')\rangle = [N_a(\omega_a) + 1]\delta(t - t'), \qquad (7)$$

$$\langle b^{in}(t)b^{in\dagger}(t')\rangle = [N_b(\omega_b) + 1]\delta(t - t'), \qquad (8)$$

$$\langle m_i^{in}(t)m_i^{in\dagger}(t')\rangle = [N_{m_i}(\omega_{m_i}) + 1]\delta(t - t'), \qquad (9)$$

$$\langle A_i^{in}(t)a^{in\dagger}(t')\rangle = [N_{A_i}(\omega_{A_i}) + 1]\delta(t - t'), \qquad (10)$$

where $N_i(\omega_i) = \{\exp[(\hbar\omega_i/k_B T) - 1]\}^{-1}$ (i= a, A_1, A_2, m_1, m_2, b) are the Bose-Einstein distribution of thermal photons, magnons and phonons.

The QLEs can be linearized in the strongly driven approximation, namely, for a, b, m_i, and A_i, their steady state amplitude $\langle O\rangle$ ($O = a, b, m_1, m_2, A_1, A_2$) is much larger than their fluctuation δO. Substitute $O = \langle O\rangle + \delta O$ into

the QLEs and ignore the higher-order terms of δO, we got the steady state solutions:

$$\langle a \rangle = \frac{\Omega_0}{i\tilde{\Delta}_{a_0} + \kappa_a}, \tag{11}$$

$$\langle m_i \rangle = \frac{(i\tilde{\Delta}_{A_i} + \kappa_{A_i})\Omega_i}{g_i^2 + (i\Delta_{m_i} + \kappa_{m_i})(i\tilde{\Delta}_{A_i} + \kappa_{A_i})}, \tag{12}$$

$$\langle A_i \rangle = \frac{g_i\langle m_i \rangle}{-\tilde{\Delta}_{A_i} + i\kappa_{A_i}}, \tag{13}$$

$$\langle b \rangle = \frac{g_{ab}|\langle a \rangle|^2 + g_{A_1b}|\langle A_1 \rangle|^2 + g_{A_2b}|\langle A_2 \rangle|^2}{\omega_b - i\kappa_b}, \tag{14}$$

where $\tilde{\Delta}_{a_0} = \Delta_{a_0} - g_{ab}(\langle b \rangle + \langle b^\dagger \rangle)$ and $\tilde{\Delta}_{A_i} = \Delta_{A_i} - g_{A_ib}(\langle b \rangle + \langle b^\dagger \rangle)$ are the effective detunings of the optical cavity and two microwave cavities. We also get the equations of the quadrature fluctuations δX_O and δY_O ($\delta X_O = (\delta O + \delta O^\dagger)/\sqrt{2}$ and $\delta Y_O = (\delta O - \delta O^\dagger)/i\sqrt{2}$, with $O = a, b, m_1, m_2, A_1, A_2$):

$$\dot{u}(t) = Au(t) + n(t), \tag{15}$$

where $u(t) = [\delta X_a(t), \ \delta Y_a(t), \ \delta X_b(t), \ \delta Y_b(t), \ \delta X_{A_1}(t), \ \delta Y_{A_1}(t), \ \delta X_{m_1}(t), \ \delta Y_{m_1}(t), \ \delta X_{A_2}(t), \ \delta Y_{A_2}(t), \ \delta X_{m_2}(t), \ \delta Y_{m_2}(t)]^T$, $n(t) = [\sqrt{2\kappa_a}X_a^{in}(t), \ \sqrt{2\kappa_a}Y_a^{in}(t), \ \sqrt{2\kappa_b}X_b^{in}(t), \ \sqrt{2\kappa_b}Y_b^{in}(t), \ \sqrt{2\kappa_{A_1}}X_{A_1}^{in}(t), \ \sqrt{2\kappa_{A_1}}Y_{A_1}^{in}(t), \ \sqrt{2\kappa_{m_1}}X_{m_1}^{in}(t), \ \sqrt{2\kappa_{m_1}}Y_{m_1}^{in}(t), \ \sqrt{2\kappa_{A_2}}X_{A_2}^{in}(t), \ \sqrt{2\kappa_{A_2}}Y_{A_2}^{in}(t), \ \sqrt{2\kappa_{m_2}}X_{m_2}^{in}(t), \ \sqrt{2\kappa_{m_2}}Y_{m_2}^{in}(t)]^T$, and

$$A = \begin{pmatrix}
-\kappa_a & \tilde{\Delta}_{a_0} & -2G_{ab}^I & 0 & 0 & 0 & 0 & 0 & 0 & 0 & 0 & 0 \\
-\tilde{\Delta}_{a_0} & -\kappa_a & 2G_{ab}^R & 0 & 0 & 0 & 0 & 0 & 0 & 0 & 0 & 0 \\
0 & 0 & -\kappa_b & \omega_b & 0 & 0 & 0 & 0 & 0 & 0 & 0 & 0 \\
2G_{ab}^R & 2G_{ab}^I & -\omega_b & -\kappa_b & 2G_{A_1b}^R & 2G_{A_1b}^I & 0 & 0 & 2G_{A_2b}^R & 2G_{A_2b}^I & 0 & 0 \\
0 & 0 & -2G_{A_1b}^I & 0 & -\kappa_{A_1} & \tilde{\Delta}_{A_1} & 0 & g_1 & 0 & 0 & 0 & 0 \\
0 & 0 & 2G_{A_1b}^R & 0 & -\tilde{\Delta}_{A_1} & -\kappa_{A_1} & -g_1 & 0 & 0 & 0 & 0 & 0 \\
0 & 0 & 0 & 0 & 0 & g_1 & -\kappa_{m_1} & \Delta_{m_1} & 0 & 0 & 0 & 0 \\
0 & 0 & 0 & 0 & -g_1 & 0 & -\Delta_{m_1} & -\kappa_{m_1} & 0 & 0 & 0 & 0 \\
0 & 0 & -2G_{A_2b}^I & 0 & 0 & 0 & 0 & 0 & -\kappa_{A_2} & \tilde{\Delta}_{A_2} & 0 & g_2 \\
0 & 0 & 2G_{A_2b}^R & 0 & 0 & 0 & 0 & 0 & -\tilde{\Delta}_{A_2} & -\kappa_{A_2} & -g_2 & 0 \\
0 & 0 & 0 & 0 & 0 & 0 & 0 & 0 & 0 & g_2 & -\kappa_{m_2} & \Delta_{m_2} \\
0 & 0 & 0 & 0 & 0 & 0 & 0 & 0 & -g_2 & 0 & -\Delta_{m_2} & -\kappa_{m_2}
\end{pmatrix} \tag{16}$$

Here $G_{ab}^R = g_{ab}Re\langle a \rangle$, $G_{ab}^I = g_{ab}Im\langle a \rangle$, $G_{A_ib}^R = g_{A_ib}Re\langle A_i \rangle$, and $G_{A_ib}^I = g_{A_ib}Im\langle A_i \rangle$ are the effective coupling rates.

Owing to the linearized dynamics of the QLEs, the Gaussian nature of the quantum noises will be preserved. Thus the steady state of the quantum fluctuations is a continuous variable (CV) six-mode Gaussian state characterized by a 12×12 covariance matrix (CM) V: $V_{ij}(t, t') = \frac{1}{2}\langle u_i(t)u_j(t') + u_j(t')u_i(t)\rangle$, which can be obtained by solving the Lyapunov equation [43, 44]:

$$AV + VA^T = -D, \tag{17}$$

where the diffusion matrix $D=diag[\kappa_a(2N_a + 1),\ \kappa_a(2N_a + 1),\ \kappa_b(2N_b + 1),$ $\kappa_b(2N_b + 1),\ \kappa_{A_1}(2N_{A_1} + 1),\ \kappa_{A_1}(2N_{A_1} + 1),\ \kappa_{m_1}(2N_{m_1} + 1),\ \kappa_{m_1}(2N_{m_1} + 1),$ $\kappa_{A_2}(2N_{A_2} + 1),\ \kappa_{A_2}(2N_{A_2} + 1),\ \kappa_{m_2}(2N_{m_2} + 1),\ \kappa_{m_2}(2N_{m_2} + 1)]$ is defined through $D_{ij}\delta(t - t') = \frac{1}{2}\langle N_i(t)N_j(t') + N_j(t')N_i(t)\rangle$

The bipartite entanglement of subsystems s_1 and s_2 can be measured by the logarithmic negativity E_N[45]:

$$E_N = \max[0, -\ln 2\tilde{\nu}_-], \tag{18}$$

where $\tilde{\nu}_- = \min eig|i\Omega P C_{s_1 s_2} P|$ ($\Omega = \bigoplus_{j=1}^{2} i\sigma_y$) is the symplectic matrix, σ_y is the y-Pauli matrix, $P = diag(1, -1, 1, 1)$, and $C_{s_1 s_2}$ is a part of the CM matrix that describes subsystems s_1 and s_2.

3 Entanglement Analysis
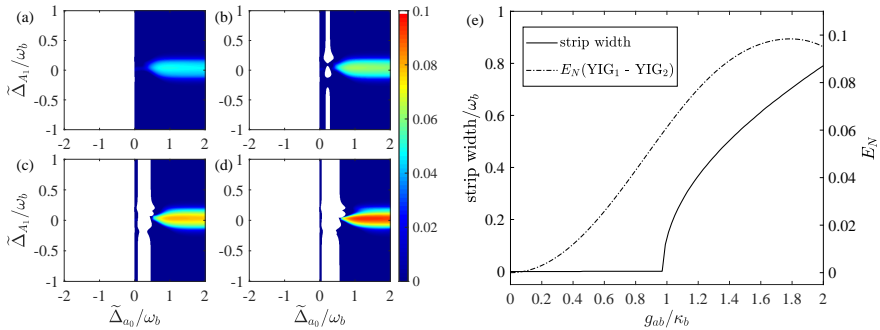
Fig. 2 (a)-(d) Steady condition of the system. The system is unsteady in the white area, while the rest part of the figure shows the entanglement E_N between two magnons m_1 and m_2 versus the effective detunings $\tilde{\Delta}_{a_0}$ and $\tilde{\Delta}_{A_1}$ (with $\tilde{\Delta}_{A_1}=\tilde{\Delta}_{A_2}=\Delta_{m_1}=\Delta_{m_2}$). Corresponding optomechanical coupling rates of the optical cavity g_{ab} are: (a) 0.8 κ_b, (b) κ_b, (c) 1.2 κ_b, (d) 1.4 κ_b. (e) The width of the vertical unsteady strip in (a)-(d) and the entanglement at the point $(\tilde{\Delta}_{a_0}, \tilde{\Delta}_{A_1}) = (\omega_b, 0)$ versus g_{ab}.

In this section, we analyze the entanglement between different components of the system in the steady state. For the complex hybrid coupling system including three driving sources, it's important to analyze the steady-state condition. The criterion of stability is that all of the eigenvalues (real parts) of the drift matrix A in Eq. (16) are negative, as a result of the Routh–Hurwitz criterion[46]. In Fig.2 we analyze the steady-state condition of the system with the following experimentally feasible parameters : $\omega_a/2\pi = 370$ THz, $(\omega_{A_1},$ $\omega_{A_2}, \omega_{m_1}, \omega_{m_2})/2\pi = (10, 10, 10, 10)$ GHz, $\omega_b/2\pi = 10$MHz, $(\kappa_a, \kappa_{A_1}, \kappa_{A_2},$ $\kappa_{m_1}, \kappa_{m_2}) = (0.4, 0.1, 0.1, 0.1, 0.1)\omega_b$, $\kappa_b/2\pi = 100$Hz, and $g_1/2\pi = g_2/2\pi =$ 1.7MHz [29, 30, 35], $\Omega_0 = 1.43 \times 10^{12}$ Hz, and $\Omega_1 = \Omega_2 = 7.13 \times 10^{14}$ Hz [30]. The result indicates that the detunings of the optical cavity and MW cavity play different roles in the steady condition. This is because the optical light

frequency leads to a higher optomechanical coupling rate than the microwave cavity[18]:

$$g_0 = Gx_{\text{ZPF}} = \omega_{\text{cav}} x_{\text{ZPF}}/L, \qquad (19)$$

where g_0 is the vacuum optomechanical coupling rate, ω_{cav} is the cavity frequency, L is the cavity length, and x_{ZPF} is the zero-point fluctuation amplitude of the mechanical oscillator. Fig.2 shows that the stability of the system is mainly determined by the optical cavity. The red detuned optical cavity ($\tilde{\Delta}_{a_0} > 0$) leads to the cooling process of the mechanical resonator and increases the robustness against temperature accordingly. An unsteady white strip appears in the red detuned area when g_{ab} is larger than the dissipation rate of the mechanical oscillator κ_b. As g_{ab} increases, the unsteady strip becomes wider. This is because the strong optomechanical coupling rate compared with the dissipation rate κ_b of the mechanical oscillator will accumulate the energy of the driving field and bring the system to an unsteady state. Fig.2 also shows that the entanglement increases with g_{ab} because the larger optomechanical coupling rate of the optical cavity leads to a stronger cooling process. Hereafter this text we take the value of g_{ab} as $1.2\kappa_b$ in order to avoid instability in the parameter regime that we investigate. According to the distribution $N_i(\omega_i) = \{\exp[(\hbar\omega_i/k_B T) - 1]\}^{-1}$, the mechanical oscillator has larger thermal noise than cavities and magnons owing to its lower eigen energy $\hbar\omega_b$. Fig.3 shows the robustness against environmental temperature. The entanglement remains constant until 60 mK and survives up to 120 mK. Fig.3 also indicates that the larger optomechanical coupling rate of the optical cavity g_{ab} increases the robustness against temperature because it enhances the cooling process and decreases the thermal noise.
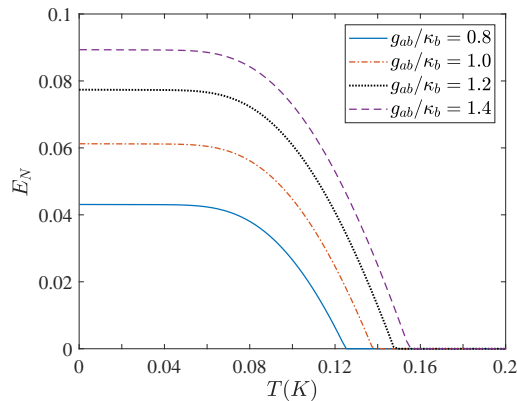
Fig. 3 The robustness of entanglement against environmental temperature. The four lines in the figure are the entanglement E_N between magnons of the two YIG spheres with different optomechanical coupling rate of the optical cavity g_{ab}. The detuning $\tilde{\Delta}_{a_0} = \omega_b$ and other detunings are zero.
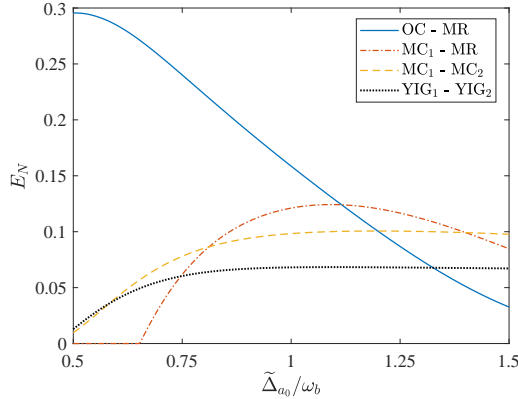
Fig. 4 Entanglement E_N versus the detuning of optical driving field $\tilde{\Delta}_{a_0}$ while $\tilde{\Delta}_{A_1} = \tilde{\Delta}_{A_2} = \Delta_{m_1} = \Delta_{m_2} = 0$. Solid line: E_N between optical cavity field and MR; dash-solid line: E_N between MW cavity (MC$_1$) field and MR; dash line: E_N between two MW cavity fields; dot line: E_N between magnons of two YIG spheres.

The components of the hybrid coupling system are individually tunable. Therefore it's important to analyze the effect of detunings on the entanglement of the system. Fig.4 indicates that the optical cavity detuned at the red sideband $\tilde{\Delta}_{a_0} = \omega_b$ materializes the best cooling process and achieves the maximum MR - MC, MC - MC, and magnon - magnon entanglements, which have been discussed earlier. Fig.5(d) shows the variation of three types of bipartite entanglements when the frequencies of the MW-driven fields change. The complementary variation of E_N(OC-MR) and E_N(MC$_1$-MC$_2$) and E_N(YIG$_1$-YIG$_2$) indicates that entanglement is transferred from the optomechanical subsystem in the optical domain to the opto-magno-mechanical subsystem in the MW domain. This phenomenon is pronounced when the MW cavities are resonantly driven because a resonantly driven cavity has the maximum average cavity photon number n_{cav} and the maximum effective optomechanical coupling strength $g = g_0 \sqrt{n_{\text{cav}}}$. The complementary variation of entanglements is demonstrated in more detail in Fig.5(a)-(c), where we assume that the MW cavity and the inside YIG sphere have the same eigenfrequency. The case that the MW cavity and the inside YIG sphere are tuned independently is discussed next.

The ferromagnetic resonant frequency of YIG spheres determined by the bias magnetic field can be tuned independently of the cavity frequency. Thus for a certain MW driving frequency, the detuning of the MW cavity $\tilde{\Delta}_{A_1}$ and the detuning of the inside YIG sphere Δ_{m_1} can be different. The variation of entanglements E_N versus $\tilde{\Delta}_{A_1}$ and Δ_{m_1} is demonstrated in Fig.6, where the detunings of the other MW cavity $\tilde{\Delta}_{A_2}$ and Δ_{m_2} remain zero. Fig.6(a) and (b) show that the maximum cavity-cavity and magnon-magnon entanglements are achieved when the driving MW field resonates with the MW cavity and the internal magnon simultaneously.
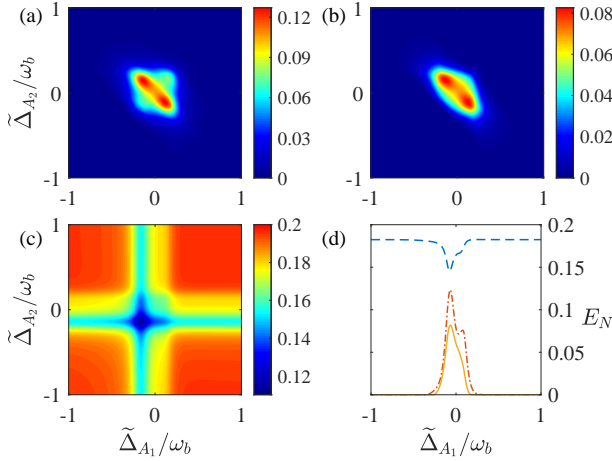
Fig. 5 (a)-(c): Entanglement E_N versus $\tilde{\Delta}_{A_1}$ and $\tilde{\Delta}_{A_2}$ while $\tilde{\Delta}_{a_0}=\omega_b$, $\tilde{\Delta}_{A_1}=\Delta_{m_1}$, and $\tilde{\Delta}_{A_2}=\Delta_{m_2}$. (a) E_N between cavity modes of MC$_1$ and MC$_2$; (b) E_N between magnons of YIG$_1$ and YIG$_2$; (c) E_N between OC and MR. (d) Entanglement E_N versus the detuning of MW driving field $\tilde{\Delta}_{A1}$ while $\tilde{\Delta}_{a_0}=\omega_b$, $\tilde{\Delta}_{A_1}=\Delta_{m_1}$, and $\tilde{\Delta}_{A_2}=\Delta_{m_2}=0.15\omega_b$. Dash-solid line: E_N(MC$_1$-MC$_2$); solid line: E_N(YIG$_1$-YIG$_2$); dash line: E_N(OC-MR).

.
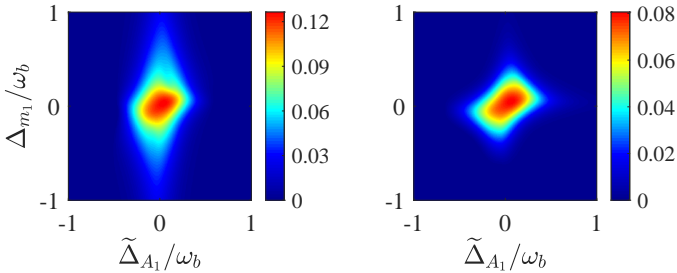
Fig. 6 Entanglement E_N versus the detuning of the MW cavity $\tilde{\Delta}_{A_1}$ and the detuning of the inside YIG sphere Δ_{m_1} while $\tilde{\Delta}_{A_2}$ and Δ_{m_2} remain zero. (a) E_N between cavity modes of MC$_1$ and MC$_2$; (b) E_N between magnons of YIG$_1$ and YIG$_2$.

Our scheme, distinguished from previous works, inserts two YIG spheres into two separate MW cavities respectively. Therefore the ferromagnetic resonate frequencies determined by the static bias magnetic fields can be tuned individually, as well as the cavity frequencies. In Fig.7 we present the variation of entanglements versus different resonate frequencies of YIG spheres while the cavity eigenfrequencies remain constant. Fig.7(a) shows the entanglement between the cavity field of MC$_1$ and the magnon of YIG$_1$. In Fig.7(a), along the x direction there is a double-peak structure of the entanglement E_N(MC$_1$-YIG$_1$). This structure is presented in detail in Fig.7(c), where the peaks exist at $\Delta_{m_1} \approx \pm 1.24 g_1$. The double-peak structure can be explained by the Rabi split. For the simple coupling model with Hamiltonian $H/\hbar =$

$\omega_{A_1} A_1^\dagger A_1 + \omega_{m_1} m_1^\dagger m_1 + g_1(A_1^\dagger m_1 + A_1 m_1^\dagger)$ and taking $\omega_{A_1} = \omega_{m_1}$ for the sake of simplicity, the Hamiltonian can be diagonalized by the supermode operators $c_\pm = (A_1 \pm m_1)$: $H/\hbar = \omega_+ c_+^\dagger c_+ + \omega_- c_-^\dagger c_-$, with supermode eigenfrequencies $\omega_\pm = \omega_{A_1} \pm g_1$. The coupling system is resonantly driven when the driving field frequency $\omega_1 = \omega_\pm$, thus the maximal local cavity-magnon entanglement is achieved at $\Delta_{m_1} \approx \pm g_1$. The deviation from $\pm g_1$ is because of the additional coupling with MR and MC_2. In addition, along the y direction in Fig.7(a) there is a dip around $\Delta_{m_2} = 0$, while in Fig.7(b) the maximal cross-cavity entanglement $E_N(MC_1\text{-}YIG_2)$ is achieved around $\Delta_{m_2} = 0$. The complementary variation of $E_N(MC_1\text{-}YIG_1)$ and $E_N(MC_1\text{-}YIG_2)$ indicates that the entanglement in the local cavity is transferred to the cross-cavity subsystem. Fig.7(d) and (e) present that the maximal entanglements $E_N(MC_1\text{-}MC_2)$ and $E_N(YIG_1\text{-}YIG_2)$ are achieved around $\Delta_{m_1} = \Delta_{m_2} = 0$, because MC_1 and MC_2 are connected by MR and the maximal entanglement $E_N(MC_1\text{-}MR)$ is achieved when $\Delta_{m_1} = 0$ (as shown in Fig.7(f)). The four types of bipartite entenglement in Fig.7 have different features when independently tuning Δ_{m_1} and Δ_{m_2}, which indicates that by independently tuning the two YIG spheres in separated MW cavities one can establish quantum channels with different entanglement properties in one system.
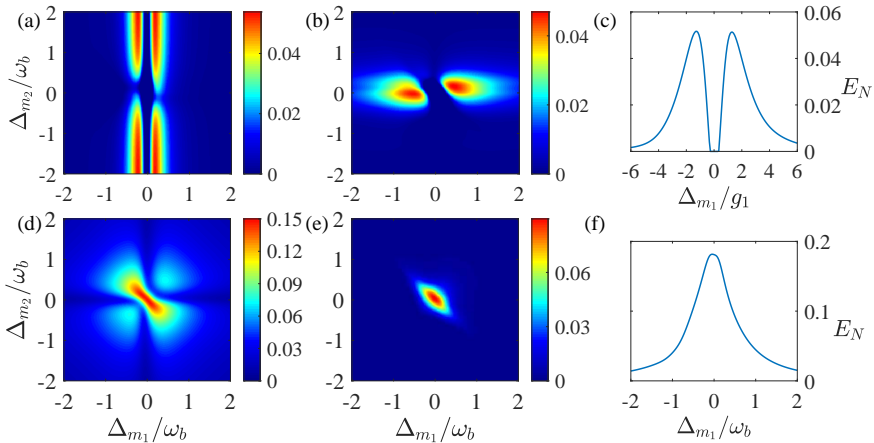
Fig. 7 Entanglement E_N versus the detuning of the two YIG spheres Δ_{m_1} and Δ_{m_2}. (a) E_N between MC_1 and YIG_1; (b) E_N between MC_1 and YIG_2; (c) The double-peak structure of $E_N(MC_1\text{-}YIG_1)$ while $\Delta_{m_2} = \omega_b$; (d)E_N between MW cavity MC_1 and MC_2; (e) E_N between YIG_1 and YIG_2; (f) E_N between MC_1 and MR while $\Delta_{m_2} = \omega_b$.

The dissipation rate of cavity is determined by the quality factor $Q = \omega_{\text{cav}}/\kappa$ while the dissipation rate of magnon is determined by the shape of YIG and the Gilbert damping process [47]. In Fig.8(a) we analyze the effect of the cavity dissipation rate κ_{A_1} while κ_{A_2} remains $0.2\omega_b$. The entanglement $E_N(MC_1\text{-}YIG_1)$, $E_N(MC_1\text{-}MC_2)$ and $E_N(YIG_1\text{-}YIG_2)$ increase at first because the increase of the steady-state solution $\langle m_1 \rangle$ according to Eq(12)

leads to the increase of the effective coupling rate. After the initial increase $E_N(\text{MC}_1\text{-YIG}_1)$, $E_N(\text{MC}_1\text{-MC}_2)$ and $E_N(\text{YIG}_1\text{-YIG}_2)$ decrease because $\langle A_1 \rangle$ decreases according to Eq(13) and decreases the effective coupling rate. Meanwhile, the entanglement $E_N(\text{MC}_2\text{-YIG}_2)$ increases because the entanglement is transferred to MC_2 as the entanglement in MC_1 decreases. The similar result is presented in Fig.8(b) where we keep $\kappa_{m_2}=0.1\omega_b$ and increase κ_{m_1}.
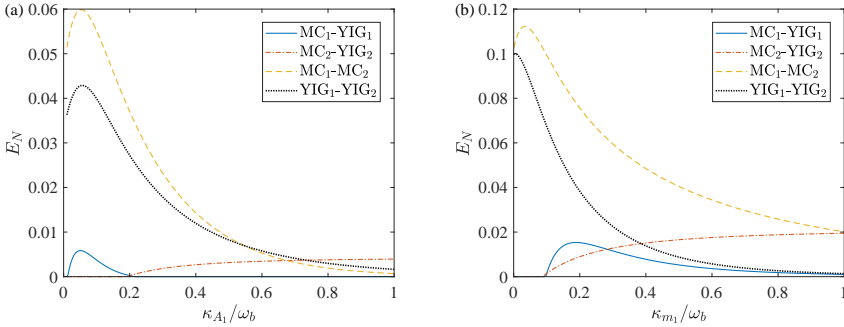
Fig. 8 (a) Entanglement E_N versus the dissipation rate κ_{A_1} of MC_1 while $\kappa_{A_2}=0.2\omega_b$. (b) Entanglement E_N versus the dissipation rate κ_{m_1} of YIG_1 sphere while $\kappa_{m_2}=0.1\omega_b$.
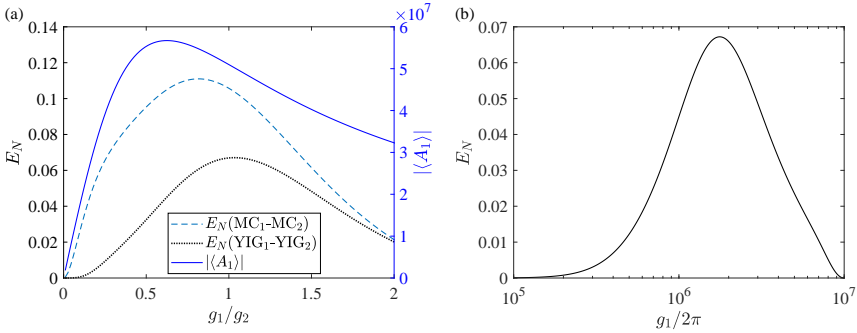
Fig. 9 Entanglement E_N versus the coupling rate between two YIG spheres. (a) g_1 varies individually while $g_2/2\pi=1.7$MHz. The variation of the steady state solution $\langle A_1 \rangle$ is shown with the right y axis. (b)$E_N(\text{YIG}_1\text{-YIG}_2)$ versus g_1 ($g_2=g_1$) which varies over a wide range.

The magnetic dipole coupling rate g_1 (g_2) between the MW cavity field and the YIG sphere is determined by the size and the position of the YIG sphere and can vary over a wide range [48], therefore g_1 and g_2 are also important parameters to be optimized. Fig.9(a) shows the variation of $E_N(\text{MC}_1\text{-MC}_2)$ and $E_N(\text{YIG}_1\text{-YIG}_2)$ versus g_1 while $g_2/2\pi=1.7$MHz. The entanglements increase at first and then begin to decrease. The variation of entanglement is determined by the effective coupling rate which is proportional to $\langle A_1 \rangle$. The variation of $\langle A_1 \rangle$ according to Eq(13) is shown in Fig.9(a). In addition, as the

ultrastrong coupling has been realized[48], we analyze the optimal value of g_1 over a wide range in Fig.9(b) while $g_1=g_2$. The result shows that entanglement exists in a wide parameter regime and the optimal parameter is $g_1 = g_2 \approx 1.7 \times 2\pi$ MHz which matches the parameter that we have chosen in this work.

4 Conclusion and Remarks

We present a novel cavity opto-magno-mechanical hybrid system to create entangled MW photons and YIG magnons, assisted by a cavity in the optical domain. Steady states are obtained by the red detuning of the optical driving field. Owing to the mechanical cooling process of the optical cavity, the system is robust against environmental temperature. We analyze the variation of entanglements versus different parameters and present the optimal condition. The two YIG spheres are embedded into two separate MW cavities respectively, therefore the ferromagnetic resonate frequencies of the two YIG spheres can be tuned independently, as well as the cavity frequencies. We analyze the individual tunability of the system and present the different entanglement features in the local-cavity and cross-cavity subsystems. The hybrid system provides a platform to generate entanglements between different physical systems. The entanglements of Gaussian states in this system represent two-mode squeezed states, which can be used to improve the precision beyond the standard quantum limit in quantum metrology [49, 50]. In addition, the entangled Gaussian states can be used in quantum information tasks such as quantum teleportation [51, 52]. The individual tunability of the separated cavities allows us to independently control the entanglement properties of different subsystems and establish quantum channels with different entanglement properties in one system, and therefore provides potential applications in quantum information tasks.

Data availability. The datasets generated and analysed during the current study are available from the corresponding author on reasonable request

References

[1] Gottesman, D., Chuang, I.L.: Demonstrating the viability of universal quantum computation using teleportation and single-qubit operations. Nature **402**(6760), 390–393 (1999). https://doi.org/10.1038/46503

[2] Knill, E., Laflamme, R., Milburn, G.J.: A scheme for efficient quantum computation with linear optics. Nature **409**(6816), 46–52 (2001). https://doi.org/10.1038/35051009

[3] Linden, N., Popescu, S.: Good dynamics versus bad kinematics: Is entanglement needed for quantum computation? Physical Review Letters **87**(4), 047901 (2001). https://doi.org/10.1103/PhysRevLett.87.047901

[4] Walther, P., Resch, K.J., Rudolph, T., Schenck, E., Weinfurter, H., Vedral, V., Aspelmeyer, M., Zeilinger, A.: Experimental one-way quantum computing. Nature **434**(7030), 169–176 (2005). https://doi.org/10.1038/nature03347

[5] Ekert, A.K.: Quantum cryptography based on bell's theorem. Physical Review Letters **67**(6), 661 (1991). https://doi.org/10.1103/PhysRevLett.67.661

[6] Lo, H.K., Ma, X., Chen, K.: Decoy state quantum key distribution. Physical Review Letters **94**(23), 230504 (2005). https://doi.org/10.1103/PhysRevLett.94.230504

[7] Hillery, M., Bužek, V., Berthiaume, A.: Quantum secret sharing. Physical Review A **59**(3), 1829 (1999). https://doi.org/10.1103/PhysRevA.59.1829

[8] Karlsson, A., Koashi, M., Imoto, N.: Quantum entanglement for secret sharing and secret splitting. Physical Review A **59**(1), 162 (1999). https://doi.org/10.1103/PhysRevA.59.162

[9] Xiao, L., Long, G., Deng, F., Pan, J.: Efficient multiparty quantum-secret-sharing schemes. Physical Review A **69**(5), 052307 (2004). https://doi.org/10.1103/PhysRevA.69.052307

[10] Bennett, C.H., Brassard, G., Crépeau, C., Jozsa, R., Peres, A., Wootters, W.K.: Teleporting an unknown quantum state via dual classical and einstein-podolsky-rosen channels. Physical Review Letters **70**(13), 1895 (1993). https://doi.org/10.1103/PhysRevLett.70.1895

[11] Bennett, C.H., Wiesner, S.J.: Communication via one-and two-particle operators on einstein-podolsky-rosen states. Physical Review Letters **69**(20), 2881 (1992). https://doi.org/10.1103/PhysRevLett.69.2881

[12] Long, G., Liu, X.: Theoretically efficient high-capacity quantum-key-distribution scheme. Physical Review A **65**(3), 032302 (2002). https://doi.org/10.1103/PhysRevA.65.032302

[13] Deng, F., Long, G., Liu, X.: Two-step quantum direct communication protocol using the einstein-podolsky-rosen pair block. Physical Review A **68**(4), 042317 (2003). https://doi.org/10.1103/PhysRevA.68.042317

[14] Pan, J., Chen, Z., Lu, C., Weinfurter, H., Zeilinger, A., Żukowski, M.: Multiphoton entanglement and interferometry. Reviews of Modern Physics **84**(2), 777 (2012). https://doi.org/10.1103/RevModPhys.84.777

[15] Raimond, J.M., Brune, M., Haroche, S.: Manipulating quantum entanglement with atoms and photons in a cavity. Reviews of Modern Physics **73**(3), 565 (2001). https://doi.org/10.1103/RevModPhys.73.565

[16] You, J., Nori, F.: Atomic physics and quantum optics using superconducting circuits. Nature **474**(7353), 589–597 (2011). https://doi.org/10.1038/nature10122

[17] Kippenberg, T.J., Vahala, K.J.: Cavity optomechanics: back-action at the mesoscale. Science **321**(5893), 1172–1176 (2008). https://doi.org/10.1126/science.1156032

[18] Aspelmeyer, M., Kippenberg, T.J., Marquardt, F.: Cavity optomechanics. Reviews of Modern Physics **86**(4), 1391 (2014). https://doi.org/10.1103/RevModPhys.86.1391

[19] Griffiths, J.H.: Anomalous high-frequency resistance of ferromagnetic metals. Nature **158**(4019), 670–671 (1946). https://doi.org/110.1038/158670a0

[20] Kittel, C.: On the theory of ferromagnetic resonance absorption. Physical Review **73**(2), 155 (1948). https://doi.org/10.1103/PhysRev.73.155

[21] Walker, L.R.: Magnetostatic modes in ferromagnetic resonance. Physical Review **105**(2), 390 (1957). https://doi.org/10.1103/PhysRev.105.390

[22] Soykal, Ö.O., Flatté, M.: Strong field interactions between a nanomagnet and a photonic cavity. Physical Review Letters **104**(7), 077202 (2010). https://doi.org/10.1103/PhysRevLett.104.077202

[23] Huebl, H., Zollitsch, C.W., Lotze, J., Hocke, F., Greifenstein, M., Marx, A., Gross, R., Goennenwein, S.T.: High cooperativity in coupled microwave resonator ferrimagnetic insulator hybrids. Physical Review Letters **111**(12), 127003 (2013). https://doi.org/10.1103/PhysRevLett.111.127003

[24] Geller, S., Gilleo, M.A.: Structure and ferrimagnetism of yttrium and rare-earth–iron garnets. Acta Crystallographica **10**(3), 239–239 (1957). https://doi.org/10.1107/S0365110X57000729

[25] Serga, A.A., Chumak, A.V., Hillebrands, B.: Yig magnonics. Journal of Physics D: Applied Physics **43**(26), 264002 (2010). https://doi.org/10.1088/0022-3727/43/26/264002

[26] Vitali, D., Tombesi, P., Woolley, M.J., Doherty, A.C., Milburn, G.J.: Entangling a nanomechanical resonator and a superconducting microwave cavity. Physical Review A **76**(4), 042336 (2007). https://doi.org/10.1103/PhysRevA.76.042336

[27] Barzanjeh, S., Vitali, D., Tombesi, P., Milburn, G.J.: Entangling optical and microwave cavity modes by means of a nanomechanical resonator. Physical Review A **84**(4), 042342 (2011). https://doi.org/10.1103/PhysRevA.84.042342

[28] Cai, Q., Liao, J., Zhou, Q.: Entangling two microwave modes via optomechanics. Physical Review A **100**(4), 042330 (2019). https://doi.org/10.1103/PhysRevA.100.042330

[29] Zhang, X., Zou, C., Jiang, L., Tang, H.X.: Cavity magnomechanics. Science Advances **2**(3), 1501286 (2016). https://doi.org/10.1126/sciadv.1501286

[30] Li, J., Zhu, S., Agarwal, G.S.: Magnon-photon-phonon entanglement in cavity magnomechanics. Physical Review Letters **121**(20), 203601 (2018). https://doi.org/10.1103/PhysRevLett.121.203601

[31] Li, J., Zhu, S., Agarwal, G.S.: Squeezed states of magnons and phonons in cavity magnomechanics. Physical Review A **99**(2), 021801 (2019). https://doi.org/10.1103/PhysRevA.99.021801

[32] Zhang, Z., Scully, M.O., Agarwal, G.S.: Quantum entanglement between two magnon modes via kerr nonlinearity driven far from equilibrium. Physical Review Research **1**(2), 023021 (2019). https://doi.org/10.1103/PhysRevResearch.1.023021

[33] Li, J., Zhu, S.: Entangling two magnon modes via magnetostrictive interaction. New Journal of Physics **21**(8), 085001 (2019). https://doi.org/10.1088/1367-2630/ab3508

[34] Yu, M., Zhu, S., Li, J.: Macroscopic entanglement of two magnon modes via quantum correlated microwave fields. Journal of Physics B: Atomic, Molecular and Optical Physics **53**(6), 065402 (2020). https://doi.org/10.1088/1361-6455/ab68b5

[35] Yu, M., Shen, H., Li, J.: Magnetostrictively induced stationary entanglement between two microwave fields. Physical Review Letters **124**(21), 213604 (2020). https://doi.org/10.1103/PhysRevLett.124.213604

[36] Yuan, H., Yan, P., Zheng, S., He, Q., Xia, K., Yung, M.: Steady bell state generation via magnon-photon coupling. Physical Review Letters **124**(5), 053602 (2020). https://doi.org/110.1103/PhysRevLett.124.053602

16   *Article Title*

[37] Tan, H., Li, J.: Einstein-podolsky-rosen entanglement and asymmetric steering between distant macroscopic mechanical and magnonic systems. Physical Review Research **3**(1), 013192 (2021). https://doi.org/10.1103/PhysRevResearch.3.013192

[38] Vidal, G., Werner, R.F.: Computable measure of entanglement. Physical Review A **65**(3), 032314 (2002). https://doi.org/10.1103/PhysRevA.65.032314

[39] Adesso, G., Serafini, A., Illuminati, F.: Extremal entanglement and mixedness in continuous variable systems. Physical Review A **70**(2), 022318 (2004). https://doi.org/10.1103/PhysRevA.70.022318

[40] Vitali, D., Gigan, S., Ferreira, A., Böhm, H., Tombesi, P., Guerreiro, A., Vedral, V., Zeilinger, A., Aspelmeyer, M.: Optomechanical entanglement between a movable mirror and a cavity field. Physical Review Letters **98**(3), 030405 (2007). https://doi.org/10.1103/PhysRevLett.98.030405

[41] Wang, Y., Zhang, G., Zhang, D., Luo, X., Xiong, W., Wang, S., Li, T., Hu, C., You, J.: Magnon kerr effect in a strongly coupled cavity-magnon system. Physical Review B **94**(22), 224410 (2016). https://doi.org/10.1103/PhysRevB.94.224410

[42] Wang, Y., Zhang, G., Zhang, D., Li, T., Hu, C., You, J.: Bistability of cavity magnon polaritons. Physical Review Letters **120**(5), 057202 (2018). https://doi.org/10.1103/PhysRevLett.120.057202

[43] Vitali, D., Gigan, S., Ferreira, A., Böhm, H., Tombesi, P., Guerreiro, A., Vedral, V., Zeilinger, A., Aspelmeyer, M.: Optomechanical entanglement between a movable mirror and a cavity field. Physical Review Letters **98**(3), 030405 (2007). https://doi.org/10.1103/PhysRevLett.98.030405

[44] Rouche, N., Habets, P., Laloy, M.: Stability Theory by Liapunov's Direct Method. Springer, New York (1977)

[45] Adesso, G., Illuminati, F.: Entanglement in continuous-variable systems: recent advances and current perspectives. Journal of Physics A: Mathematical and Theoretical **40**(28), 7821 (2007). https://doi.org/10.1088/1751-8113/40/28/s01

[46] DeJesus, E.X., Kaufman, C.: Routh-hurwitz criterion in the examination of eigenvalues of a system of nonlinear ordinary differential equations. Physical Review A **35**(12), 5288 (1987). https://doi.org/10.1103/PhysRevA.35.5288

[47] Rameshti, B.Z., Kusminskiy, S.V., Haigh, J.A., Usami, K., Lachance-Quirion, D., Nakamura, Y., Hu, C.-M., Tang, H.X., Bauer, G.E., Blanter,

Y.M.: Cavity magnonics. Physics Reports **979**, 1–61 (2022). https://doi.org/10.1016/j.physrep.2022.06.001

[48] Zhang, X., Zou, C., Jiang, L., Tang, H.X.: Strongly coupled magnons and cavity microwave photons. Physical Review Letters **113**(15), 156401 (2014). https://doi.org/10.1103/PhysRevLett.113.156401

[49] Zhang, Z., Duan, L.: Quantum metrology with dicke squeezed states. New Journal of Physics **16**(10), 103037 (2014). https://doi.org/10.1088/1367-2630/16/10/103037

[50] Anisimov, P.M., Raterman, G.M., Chiruvelli, A., Plick, W.N., Huver, S.D., Lee, H., Dowling, J.P.: Quantum metrology with two-mode squeezed vacuum: parity detection beats the heisenberg limit. Physical review letters **104**(10), 103602 (2010). https://doi.org/10.1103/PhysRevLett.104.103602

[51] Wang, X.-B., Hiroshima, T., Tomita, A., Hayashi, M.: Quantum information with gaussian states. Physics reports **448**(1-4), 1–111 (2007). https://doi.org/10.1016/j.physrep.2007.04.005

[52] Braunstein, S.L., Van Loock, P.: Quantum information with continuous variables. Reviews of modern physics **77**(2), 513 (2005). https://doi.org/10.1103/RevModPhys.77.513